

Two epoch spectro-imagery of FS Tau B outflow system^{★,★★,★★★}

T. A. Movsessian¹, T. Yu. Magakian¹, and A. N. Burenkov²

¹ Byurakan Astrophysical Observatory NAS Armenia, Byurakan, Aragatsotn Province 0213, Armenia
e-mail: tigmov@bao.sci.am; timag@sci.am

² Special Astrophysical Observatory, N.Arkhыз, Karachaevo-Cherkesia 369167, Russia
e-mail: ban@sao.ru

Received 4 April 2019 / Accepted 15 May 2019

ABSTRACT

Context. Herbig–Haro (HH) flows exhibit a large variety of morphological and kinematical structures such as bow shocks, Mach disks, and deflection shocks. Both proper motion (PM) and radial velocity investigations are essential to understand the physical nature of such structures.

Aims. We investigate the kinematics and PM of spectrally separated structures in the FS Tau B HH flow. Collating these data makes it possible to understand the origin of these structures and to explain the unusual behavior of the jet. Besides, the study of emission profiles in the associated reflection nebulae allows us to consider the source of the outflow both from edge-on and pole-on points of view.

Methods. We present the data obtained with the 6 m telescope at the Special Astrophysical Observatory of the Russian Academy of Sciences using the SCORPIO multimode focal reducer with a scanning Fabry–Perot interferometer. Two epochs of the observations of the FS Tau B region in H α emission (2001 and 2012) allowed us to measure the PM of the spectrally separated inner structures of the jet.

Results. In addition to already known emission structures in the FS Tau B system, we discover new features in the extended part of the jet and in the counter-jet. Moreover, we reveal a new HH knot in the HH 276 independent outflow system and point out its presumable source. In the terminal working surface of the jet, structures with different radial velocities have PMs of the same value. This result can be interpreted as the direct observation of bow-shock and Mach disk regions. A bar-like structure, located southwest from the source demonstrates zero PM and can be considered as one more example of deflection shock. An analysis of H α profiles in the reflection nebulae R1 and R3 indicates the uniqueness of this object, which can be studied in pole-on and edge-on directions simultaneously.

Key words. stars: pre-main sequence – stars: individual: FS Tau B – ISM: jets and outflows – Herbig–Haro objects

1. Introduction

Variable star FS Tau (Haro 6-5, HBC 383) (Haro et al. 1953) is located in the Taurus dark cloud on the distance of 140–145 pc (Kenyon et al. 2008). It is surrounded by reflection nebulae of various sizes and shapes. About 20'' to the west from this star, on the axis of bright reflection nebula, one of the first Herbig–Haro (HH) jets (HH 157) was discovered (Mundt et al. 1984). This jet includes various morphological structures and is narrowing with the distance in an uncommon way (Mundt et al. 1991). The star-like knot, located near the apex of this nebula, was recognized as the source of the outflow and designated as Haro 6-5 B (HBC 381, FS Tau B) (Mundt et al. 1984).

Long-slit spectroscopy revealed the bipolarity of the HH 157 outflow and confirmed the reflection nature of the conical nebula in its apex (Mundt et al. 1987). Low absolute values of radial velocities, observed both in the jet and the counter-jet, point to the flow orientation that is close to the plane of the sky (Eisloffel & Mundt 1998). Further observations with *Hubble* Space Telescope (HST) revealed the compact bipolar

reflection nebula, similar to HH 30, in the FS Tau B location (Ray et al. 1996; Krist et al. 1998). The source itself is not visible directly because it is located behind the dust lane, which bisects this nearly edge-on oriented nebula (Krist et al. 1998; Padgett et al. 1999; Woitas et al. 2002). The FS Tau B system, especially its circumstellar disk, became the subject of recent studies in various wavelength ranges (Yokogawa et al. 2001; Kirchschlager et al. 2016). It is worth noting that in vicinity of FS Tau B a bipolar molecular outflow was also detected (Mottram et al. 2017), which is about 2' in length. Its blueshifted and redshifted lobes coincide with the jet and counter-jet parts of FS Tau B HH 157 optical outflow, respectively.

The complex inner morphology of jets from young stellar objects was effectively revealed by scanning Fabry–Perot interferometer (FPI) observations, which can successfully separate structures with high and low radial velocity (Morse et al. 1992, 1993; Hartigan et al. 2000; Movsessian et al. 2007). This observational technique provides high spectral resolution data with full two-dimensional coverage in the large field of view. Notwithstanding the small spectral range, which allows us to investigate only one emission line, it is a very powerful method to study extended emission objects such as HH objects and optical jets.

In fact, only spectro-imagery allowed for the revelation of the morphology of different kinematical structures not only in the working surfaces but in the inner structures of jets as well (Morse et al. 1993; Hartigan et al. 2000; Movsessian et al. 2000, 2007, 2009). For a better understanding of the physical nature of such

* The channel movie is available at <https://www.aanda.org>

** Reduced datacubes (FITS files) are only available at the CDS via anonymous ftp to [cdsarc.u-strasbg.fr](ftp://cdsarc.u-strasbg.fr) (130.79.128.5) or via <http://cdsarc.u-strasbg.fr/viz-bin/qcat?J/A+A/627/A94>

*** This work is based on observations conducted with the 6 m telescope of the Special Astrophysical Observatory of the Russian Academy of Sciences carried out with the financial support of the Ministry of Science and Higher Education of the Russian Federation.

structures it is very important to combine the radial velocity data with proper motions (PM). We developed a new method of PM measurement for jet structures with various radial velocity using two epochs of scanning FPI observations. It provides both the spectral separation of the structures by their radial velocity and the measurement of their PM. It was already tested on HL Tau jet, for which we revealed internal structures with surprisingly different radial velocities but with the same PM (Movsessian et al. 2007, 2012).

The present paper extends this approach to the FS Tau B HH outflow system. We focus on the full kinematical picture of various emission structures inside the jet and its working surface. In addition, in the course of our study dramatic changes of H α profiles in the jet source and its reflection nebula have been found; we discuss these changes as well.

2. Observations and data reduction

Observations were carried out in the prime focus of the 6 m telescope of Special Astrophysical Observatory (SAO) of the Russian Academy of Sciences in two epochs: 19 September 2001 and 22 November 2012 in good seeing conditions of about 1". We used an FPI placed in the parallel beam of the SCORPIO focal reducer. This device is described by Afanasiev & Moiseev (2005) and the SCORPIO capabilities in the scanning FPI observational mode are described by Moiseev (2002).

The detector used during the first epoch of observations was a TK1024 1024 \times 1024 pixel CCD array. Observations were performed with 2 \times 2 pixel binning to reduce the readout time, so 512 \times 512 pixel images were obtained in each spectral channel. The field of view was 4.80' and the scale 0.56" per pixel (after binning).

The scanning interferometer, used in these observations, was Queensgate ET-50. This instrument operates in the 501st order of interference at the H α wavelength and provides a spectral resolution of $FWHM \approx 0.8 \text{ \AA}$ (or $\approx 40 \text{ km s}^{-1}$) for a range of $\Delta\lambda = 13 \text{ \AA}$ (or $\approx 590 \text{ km s}^{-1}$) free from order overlapping. The number of spectral channels was 36 and the size of a single channel was $\Delta\lambda \approx 0.36 \text{ \AA}$ ($\approx 16 \text{ km s}^{-1}$). The exposure time was 160 s per channel and the total exposure time was 96 min.

During the second epoch observations the detector was an EEV 40-42 2048 \times 2048 pixel CCD array. The observations were performed with 4 \times 4 pixel binning and therefore 512 \times 512 pixel images were obtained in each spectral channel. The field of view was 6.1' for a scale of 0.72" per pixel (after binning). In both epochs an interference filter with $FWHM = 15 \text{ \AA}$ centered on the H α line was used for pre-monochromatization (Moiseev & Egorov 2008).

The scanning interferometer was ICOS FPI operating in the 751st order of interference at the H α wavelength, providing spectral resolution of $FWHM \approx 0.4 \text{ \AA}$ (or $\approx 20 \text{ km s}^{-1}$) for a range of $\Delta\lambda = 8.7 \text{ \AA}$ (or $\approx 390 \text{ km s}^{-1}$) free from order overlapping. The number of spectral channels was 40 and the size of a single channel was $\Delta\lambda \approx 0.22 \text{ \AA}$ ($\approx 10 \text{ km s}^{-1}$). The exposure time was 200 s per channel and the total exposure time was 133 min.

We reduced our interferometric observations using the software developed at the SAO (Moiseev 2002; Moiseev & Egorov 2008) and the ADHOC software package¹. After primary data reduction, subtraction of night-sky lines, and wavelength calibration, the observational material represents so called data

¹ The ADHOC software package was developed by J. Boulesteix (Marseille Observatory) and is publicly available on the Internet.

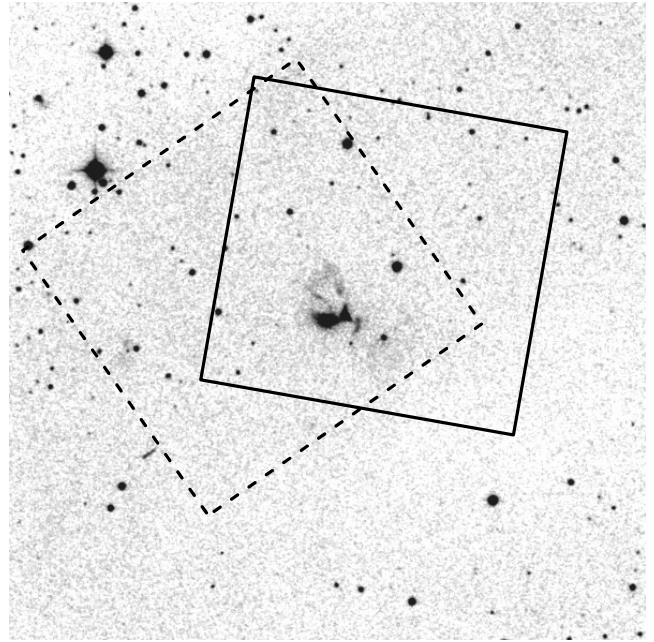


Fig. 1. 10' \times 10' DSS-2 image of the FS Tau B outflow system. Regions, covered by FPI, are outlined with rectangles, solid for 2001 and dashed for 2012 epochs.

cubes. The corrections of data for telescope guiding errors and for variations of atmospheric transparency and seeing were performed by a method, described by Moiseev (2002), which significantly decreases their influence. Final data cubes were subjected to optimal data filtering, which included Gaussian smoothing over the spectral coordinate with $FWHM = 1.5$ channels and spatial smoothing by a two-dimensional Gaussian with $FWHM = 2-3$ pixels.

Using these data cubes, we spectrally separated the structures in the outflow system. Then PMs were measured for the selected structures using observations in both epochs. For the PM estimation a method of two-image optimal offset computation by means of cross-correlation was used (realized as procedure by F. Varosi and included in IDL astronomy library²).

3. Results and discussion

3.1. Overview

In Fig. 1 the fields covered by SCORPIO camera during FPI observations in 2001 and 2012 are outlined on the 10' \times 10' image of DSS-2 red plate. As can be seen, the field, observed in 2012, includes more structures of the outflow system; moreover, it has a deeper limit, allowing the detection of many faint features. In addition to emission features, the field includes the bright cone-shaped reflection nebula R1, the star-like reflection nebula R3 near the position of the source, and the reflection nebula R2 and cavity walls seen in reflected light (see Eislöffel & Mundt 1998, Fig. 8). In the outflow system the central part of the jet as well as the terminal shock region with knots L and K, and the northeastern extension of the flow with knots M and N (nomenclature of Eislöffel & Mundt 1998) are covered (Fig. 2). Moreover, we discovered an additional linear emission structure connected with a faint bow-shaped wing designated as M2

² <https://idlastro.gsfc.nasa.gov/>

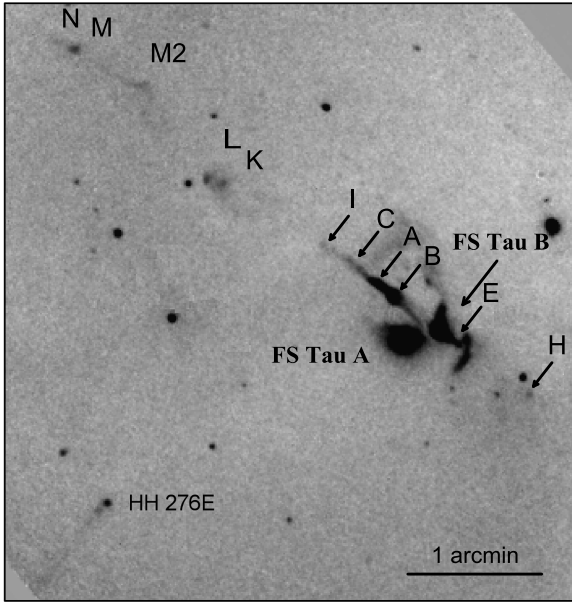


Fig. 2. Image of the field, covered by FPI observations in 2012, in the $H\alpha$ line integrated over all channels. Emission structures in the HH 157 flow are denoted using the nomenclature of Eislöffel & Mundt (1998). Newly discovered knot M2 and Herbig–Harro object HH 278E are shown as well.

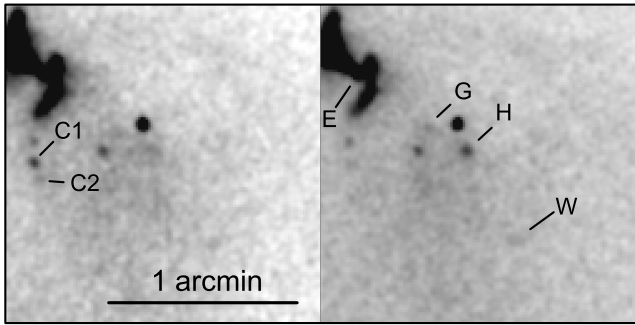


Fig. 3. Southwestern side of FS Tau B flow. The *left panel image* corresponds to the radial velocity of $+39 \text{ km s}^{-1}$ and the *right image* to $+79 \text{ km s}^{-1}$. Emission knots are indicated using the nomenclature of Eislöffel & Mundt (1998); also the newly discovered knot W is shown.

between the bow shock and the knot M, which is barely visible on the [S II] image of Eislöffel & Mundt (1998).

In the counter-jet we detected the emission knots E (near the R3 star-like nebula), G, and H as well as the more distant faint knot, which we denote as W. Alongside this linear chain of knots, C1 and C2 knots (see Fig. 3) are also visible, but they probably do not belong to the FS Tau B counter-jet flow.

The field of view also includes the independent outflow HH 276 (Eislöffel & Mundt 1998). In this system we found an additional bright knot, designated as HH 276 E, which traces this flow in the southeastern direction.

We estimate radial velocities and PM for various structures of FS Tau B jet, which were visible in both data sets, and compared these with the values presented by Eislöffel & Mundt (1998). It should be noted that our observations were separated by about 11 yr, and this time interval is longer than the cooling time of shocked structures. Indeed we detect some morphological changes in several knots. Investigation of the emission lines profiles near the source (R3 reflection nebula) and in the bright

reflection nebula R1 is of a special interest (Movsessian et al. 2014). Below we discuss all these results in detail.

3.2. Morphology of the HH 157 flow inner structures

The appearance of certain parts of the HH 157 flow strongly depends on absolute radial velocity, which can be seen from the images in various channels obtained during our 2012 observations (Fig. 4). The main jet is wider in low velocity channels compared with the higher velocity channels, similar to the jet from HL Tau (Movsessian et al. 2007). With better clarity these changes can be seen in a channel movie, which is available [online](#). Considering that the jet consists of a number of small internal working surfaces, this feature may have two causes. On the one hand, each internal working surface includes a compact high velocity Mach disk and low velocity extended bow shock. On the other hand, in each bow-shock radial velocities are maximal near its apex.

Most prominent feature in the FS Tau B jet is the bow-shaped knot B (see Fig. 2 for details). A linear emission structure extends from this bright knot toward the source; however, it does not coincide with the axis of the jet. The nature of this structure is discussed below. The bow-shock region (knots K and L) demonstrates most significant changes in morphology with velocity (Fig. 4). In high radial velocities both condensations appear as two compact knots, while in lower velocities they turn into separate bow-shaped structures. More distant parts of the flow (knots N, M, and newly discovered M2) do not undergo noticeable variations depending on velocity. This can be explained by the decrease of ambient medium and flow density ratio, which results in a bright bow shock and a very faint Mach disk (Hartigan 1989).

A narrow counter-jet, ending with relatively bright knot E, is visible near the source in positive radial velocities while jet as whole has negative velocity. The counter-jet points in the direction of knot H. It should be noted that the counter-jet, knots G, H, and the newly discovered knot W, are better seen in the channels near $+80 \text{ km s}^{-1}$ velocity, but knots C1 and C2 differ by much lower velocity ($+40 \text{ km s}^{-1}$), and their relation to counterflow is doubtful (see Fig. 3).

Finally, the unusual appearance of the FS Tau B jet, which narrows along with the distance from the source, can be a result of exceptionally bright and extended bow-shaped knot B. Thus, it could be not associated with the variations in the flow collimation.

3.3. Radial velocities

Because of higher spectral resolution, we concentrate on the radial velocities, obtained in the second epoch; in any case, the differences of radial velocities between two epoch observations do not exceed 5 km s^{-1} for knot B and are lower than 2 km s^{-1} for other knots. To compare our results with the previous measurements, obtained by means of long-slit spectroscopy (Eislöffel & Mundt 1998), we generated a pseudo-slit, which is oriented along the axis of the jet on the base of the data cube obtained in 2012. Figure 5 shows a jet image in $H\alpha$ emission and position-velocity (PV) diagram. This diagram only covers the central part of the jet near the source and does not include bow shock because the jet axis does not point toward the bow apex. Intensities in the PV diagram are presented in the logarithmic scale because of their strong variations along the jet.

From the PV diagram it is obvious that the absolute radial velocity increases from the source up to the knots B and A.

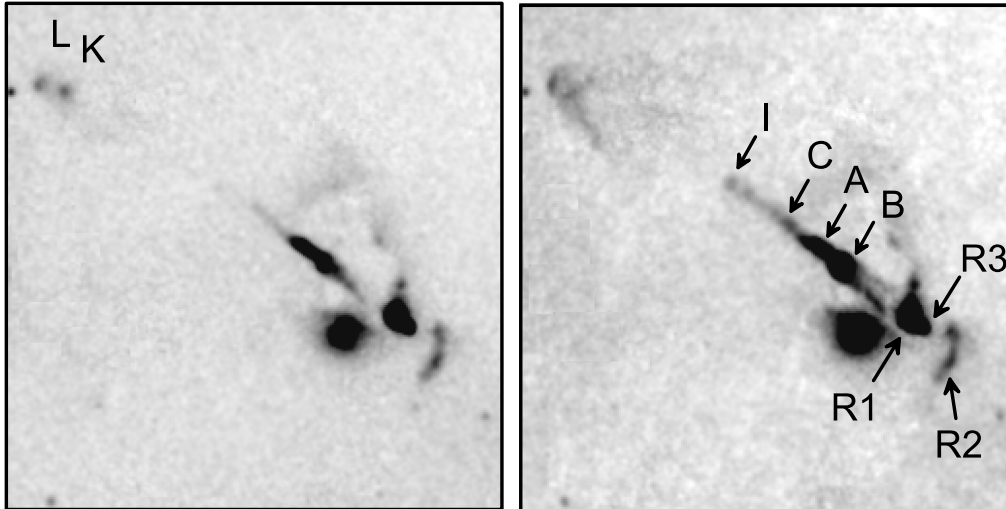


Fig. 4. Two channels from the observations with FPI in 2012, which show the variations in the morphology of FS Tau B jet, depending on heliocentric radial velocities; the *left panel* corresponds to -77 km s^{-1} and the *right one* to -36 km s^{-1} .

Beyond this bright central part of the jet and up to the knot I radial velocity exhibits low changes. There are evident signs of the existence of low velocity wings in $H\alpha$ profiles in the positions of knot B and especially knot A.

Our data are in good accordance with measurements of Eislöffel & Mundt (1998), especially for the brightest knots, confirming the low absolute values of radial velocities in the jet and counter-jet. The disagreement between old and new data, however, increases toward the end of jet. The probable reason is that the jet is curved and during the observations of Eislöffel & Mundt (1998) the long slit of spectrograph missed its end.

Therefore, we slightly changed the orientation of pseudo-slit to extend the intensity map and PV diagram of HH 157 flow to its bow-shock region, defined by knots K and L. Results are shown in Fig. 6, which is similar to Fig. 5. The existence of two velocity components in the knot K is obvious. As we already discussed in the previous section, the low velocity component represents bow-shaped structure, while high velocity component is produced in the compact knot. In knot L the split in velocity is not so evident but the low velocity wing is clearly visible. Full data about heliocentric radial velocities of the knots, indicated on the PV diagram and in the extended parts of the flow, are gathered in Table 1.

3.4. Proper motions

We measured PM for all the jet structures that were detectable in the images of both epochs. The results are presented in Table 1: i.e., distances for each knot, measured from the center of R3 reflection nebula; values of tangential velocities, computed for the distance of 150 pc for easy comparison with the data of Eislöffel & Mundt (1998); PAs; and radial velocities.

The high values of PM of knots in the FS Tau B jet were already known from previous studies; nevertheless, the data presented in this work are of additional interest because they refer to the knots selected in the same velocity channels. Moreover, in the cases in which inner structures undergo strong morphological changes depending on the radial velocity, we present PM values for these features in both velocity channels. To achieve a better comparison of morphological details in these cases, we performed the rebinning of the second epoch data cube to bring both of them to the same velocity steps. In general our PM measurements are in good accordance with the values presented by Eislöffel & Mundt (1998).

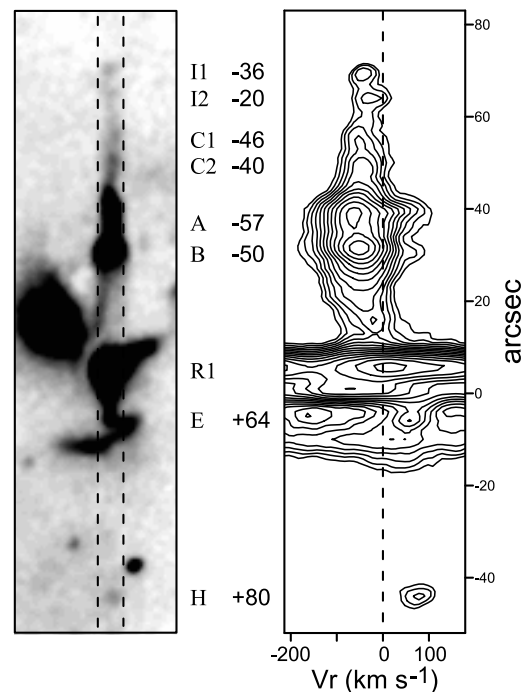


Fig. 5. Monochromatic $H\alpha$ image of the FS Tau B jet and the orientation of pseudo-slit (*left*) and corresponding PV diagram. Zero velocity is shown by a dashed line (*right*). Knots and their radial velocities are indicated between the panels.

The PM vectors for the various structures in the HH 157 jet and the counter-jet are shown separately in Fig. 7. To achieve better representability the images in both frames of Fig. 7 were obtained by integration of channels, corresponding to blueshifted and redshifted ranges of $H\alpha$ emission.

Figure 8 shows isolines of integrated $H\alpha$ images of FS Tau B outflow for both epochs; the shifts of selected knots are indicated by arrows. The high PM of knot B is obvious. It results in the striking “sliding” of knot B along the jet. Knot I2, which is barely visible on the 2001 image and was not detected at all in the images of Eislöffel & Mundt (1998), is well visible in 2012.

As was described previously, the working surface of the jet contains two separate structures designated as knots K and L. Their morphology strongly changes with radial velocity. We

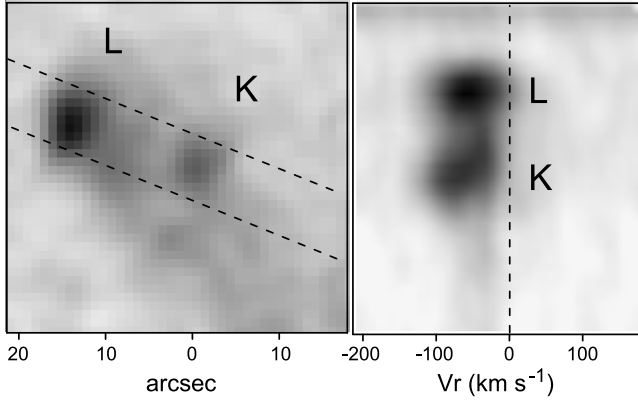


Fig. 6. Monochromatic image of the FS Tau B jet bow-shock part and pseudo-slit orientation (*left*) and corresponding PV diagram (*right*). North is up.

Table 1. Proper motions and radial velocities of knots in the FS Tau B outflow.

Knot	Distance ^(a) (arcsec)	$V_{\text{tan}}^{(b)}$ (km s^{-1})	V_{tan} (arcsec yr^{-1})	PA (deg)	V_r (km s^{-1})
B	31.5	395 ± 30	0.62	46	-50
A	38.7	231 ± 35	0.37	41	-57
C2	48.5	–	–	–	-40
C1	53.9	248 ± 25	0.39	55	-46
I2	63.5	–	–	–	-20
I1	68.5	279 ± 22	0.44	56	-36
K _{high vel}	120.2	360 ± 23	0.55	55	-77
K _{low vel}	120.8	–	–	–	-30
L _{high vel}	127.7	285 ± 25	0.42	58	-60
L _{low vel}	128.8	290 ± 36	0.46	56	-30
M2	176	–	–	–	-30
M	209	–	–	–	-45
N	220	–	–	–	-45
E	5.9	180 ± 26	0.29	220	+65
G	31.7	–	–	–	+78
H	44.7	160 ± 20	0.25	230	+80

Notes. ^(a)Distances of knots are measured on 2012 image, taking the R3 bright knot as a zero point. ^(b)Tangential velocities correspond to 150 pc as a distance of the flow.

tried to measure PM of high and low velocity structures in these knots separately. But the detection limit in 2001 observations was lower, which makes the low velocity structure in K knot blurred and poorly pronounced. Therefore its PM was not possible to measure with sufficient precision. In comparison, in knot L both high and low velocity structures are clearly outlined and measurable. PM of these velocity structures are the same, although the radial velocities are very different. This result is consistent with analogous measurements of knots in the HL Tau jet (Movsessian et al. 2012).

Different radial velocity structures in the knots of the jets and terminal working surfaces are usually interpreted as two principal shocks regions: a “reverse shock (Mach disk)”, which decelerates the supersonic flow, and a “forward shock”, which accelerates the material with which it collides (Hartigan 1989). The morphologies of these structures are very different: reverse shock appears as a compact knot while forward shock is represented by a bow-shaped extended structure.

Taking this approach into account, it is possible to obtain more precise estimations for the orientation angle of flows. Since

in the reverse shock region the ratio ζ between the pattern speed of the knots and the flow speed of the jet particles is equal to one (i.e., $v_{\text{pattern}} = v_{\text{flow}}$), the orientation angle can be calculated by the ratio of v_{rad} to v_{tan} (Eislöffel & Mundt 1992). To apply this method for the FS Tau B flow, we chose knot L, for which both shock regions are clearly divided. Using tangential and radial velocities of the high velocity structure of the knot L, we found that its inclination to the plane of the sky and its spatial velocity are equal to 12° and 300 km s^{-1} , respectively. On the other hand, these values should vary with the distance from the source due to precession.

Another interesting feature in the FS Tau B flow is the bar-shaped structure with length about $20''$ mentioned above; this structure starts at a point located to the northeast from the source. In 2012 this structure is a little disturbed by the fast-moving B knot, but the structure is clearly visible in 2001. Therefore, we demonstrate its appearance in 1987 on the $H\alpha$ image of FS Tau B, provided to us by J. Eislöffel, and in the monochromatic image obtained with FP etalon in 2001 (Fig. 9). It can be easy concluded that the bar-shaped structure appears stationary and, as in the case of HH 47, can be interpreted as a deflection shock region (Hartigan et al. 2005, 2011).

Finally, the unusual appearance of the FS Tau B jet, which narrows with the distance from the source, could be a result of the exceptionally bright and extended bow-shaped knot B. Thus, the narrowing of the jet is probably not related to the variations in the flow collimation (Mundt et al. 1991).

3.5. Source and reflection nebula R1

Our data cubes allow us to study the $H\alpha$ emission profiles not only in the spectra of the star and of its directed outflow, but also in the various reflection nebulae associated with this system. To be more precise, we must note that the star FS Tau B itself is totally obscured, as was shown by Stapelfeldt et al. (1997), and its optical radiation cannot be observed directly. The bright stellar-like knot (R3), located to the northeast from the source, probably represents the upper surface of the circumstellar disk seen edge-on. Further observations with Wide Field Planetary Camera 2 on the HST revealed the structure of the source in more detail. Images show that the source of a bipolar jet appears to illuminate a compact, bipolar nebula which is assumed to be an edge-on protostellar disk similar to HH 30 (Ray et al. 1996; Krist et al. 1998).

To study wide $H\alpha$ line profiles in the reflection nebulae we used first epoch observations, which covered wider spectral range. As can be seen from Fig. 10 and the PV diagram (Fig. 5), the $H\alpha$ line profile, which corresponds to R3 reflection nebula, shows broad emission. In contrast, the averaged profile in the R1 nebula is split into two components. It should be noted, that the emission profile in the position of R3 nebula is typical for the edge-on T Tau stars (Appenzeller et al. 2005) and the profile in the R1 nebula is similar to the majority of classical T Tau stars. In our opinion, reflection nebula R1 works as a mirror via which we observe the light from the source from pole-on point of view; this contrasts with R3 nebula through which we observe an edge-on system. The situation is somewhat similar to the geometry in the R Mon+NGC 2261 system (Jones & Herbig 1982).

The profile of $H\alpha$ emission, observed in R1 reflection nebula, consists of two peaks: first peak is a wide triangular-shape line, little shifted in the red range and the second peak is a strongly blueshifted emission with radial velocity of about -200 km s^{-1} . The first emission peak can be explained by assuming magnetospheric accretion with high accretion rate of about $10^{-7} M_\odot \text{ yr}^{-1}$

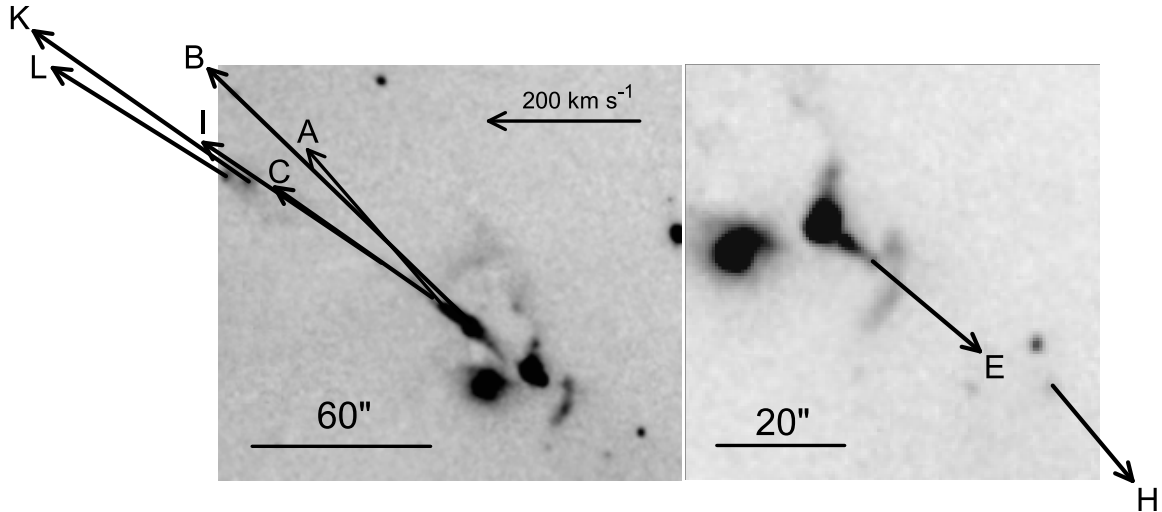


Fig. 7. Monochromatic images of the FS Tau B jet and the counter-jet with superposed PM vectors of individual knots. Images are obtained by integrating over the blueshifted (*left*) and redshifted (*right*) components of $H\alpha$ emission.

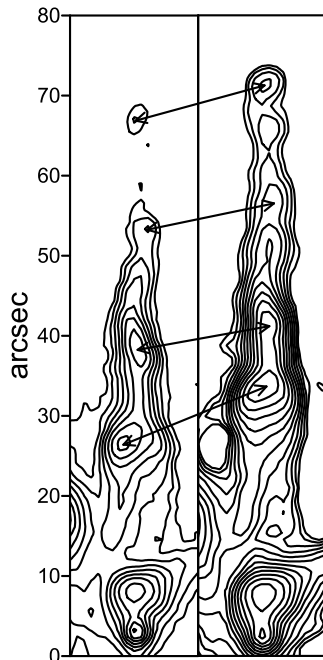


Fig. 8. Monochromatic images of FS Tau B jet in 2001 (*left*) and 2012 (*right*). Arrows connect the same knots in both epochs.

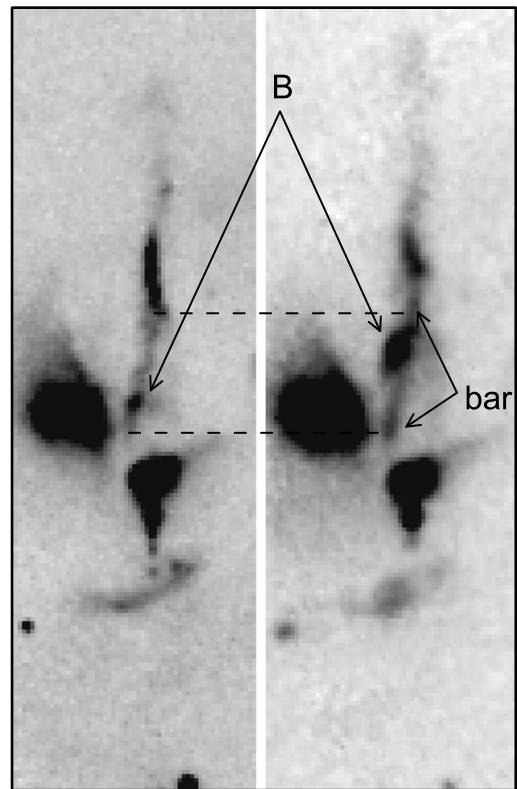


Fig. 9. $H\alpha$ image of the FS Tau B jet obtained by Eislöffel & Mundt (1998) in 01.01.1987 (*left*) and monochromatic image of the FS Tau B jet in low radial velocity channel (-15 km s^{-1}) obtained in 19.09.2001 (*right*). Fast-moving knot B and the stationary bar are denoted.

(Kurosawa et al. 2006). The division of emission profile could be produced by absorption in disk wind (Kurosawa et al. 2006), but in this specific case the stellar emission (i.e., first peak) is symmetric and the velocity of blueshifted second peak is too high in comparison with the model. In our opinion, the blueshifted peak is created by high velocity outflow that is observed close to its axis (via the point of view in R1 nebula).

The situation completely differs in R3 nebula. Considering the full $H\alpha$ profile, we can see that it consists of two blended emission components, one of which has nearly zero velocity and the other is blueshifted to about -70 km s^{-1} ; it should be noted that this shift is very close to the velocity of the jet in FS Tau B flow. We suggest that zero velocity component has the same origin as in R1 nebula (but is more faint) and probably corresponds to stellar emission, obscured by circumstellar disk or torus in contrast with the more extended emission of the outflow. On

the other hand, the width of blueshifted emission line exceeds the width of the jet emission much more. We suggest that this component corresponds to the base of the jet where the opening angle of flow is wider in comparison with the jet itself. Such large values for the initial opening angle of several HH jets were estimated from high spatial resolution images obtained with HST (Ray et al. 1996).

It is necessary to note that these assumptions consider a simple single light scattering on the dust in the reflection nebulae.

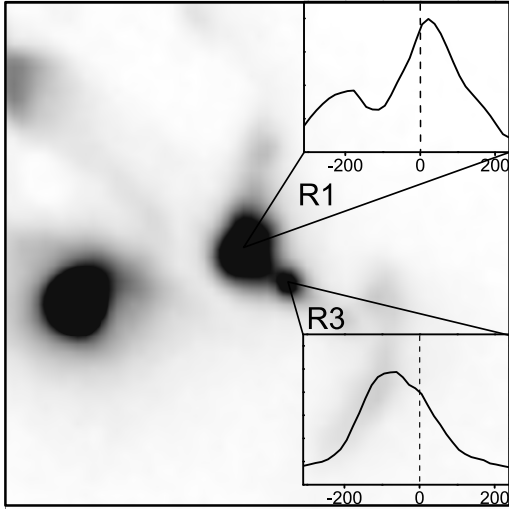


Fig. 10. Integrated $H\alpha$ profiles observed in R1 and R3 reflection nebulae. Radial velocities are indicated in the boxes with profiles.

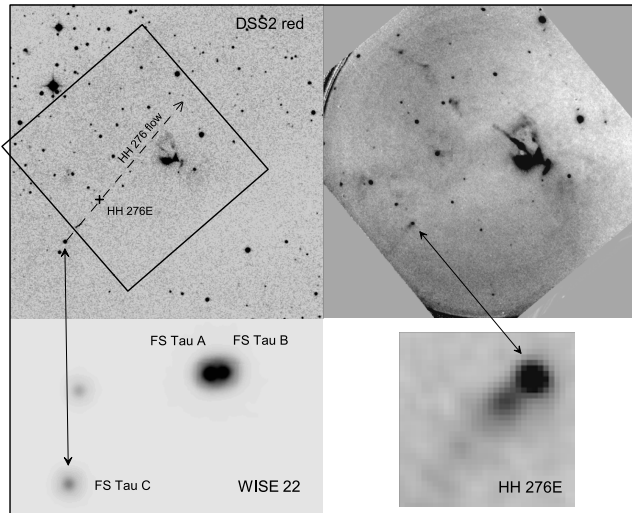


Fig. 11. Positions of the newly discovered HH 276E object and the proposed source of HH 276 flow (FS Tau C). The *top left panel* shows their location on the DSS-2 red image and the *bottom left* shows the WISE survey $22\ \mu\text{m}$ image. The *top right panel* repeats the image, presented in Fig. 2, and the *bottom right* shows the enlarged image of HH 276E.

More complicated effects, such as variable extinction or circumstellar shadowing, are not taken into account. They probably can change the relative intensities of the emission components.

3.6. HH 276 outflow system

This independent outflow was discovered by Eislöffel & Mundt (1998) as a diffuse emission tail, almost perpendicular to FS Tau jet. The length of this flow is about $150''$ and includes several faint knots. The source of this flow was not known, but an assumption was made that it should be located in northwestern direction. It was preliminary designated as FS Tau C (Eislöffel & Mundt 1998).

As mentioned above, we found a bright emission object in southeastern part of the studied field. This object consists of two knots and has a faint tail that is well aligned with the axis of HH 276 flow. This object, with coordinates $RA = 04^{\text{h}} 22^{\text{m}} 12^{\text{s}}$,

$Dec = +26^{\circ} 56' 19''$ (2000), definitely comprises a part of HH 276 flow, and we designated the object as HH 276E (Fig. 11). Thus, the whole length of HH 276 outflow system extends to about $200''$. The radial velocity of this outflow is about $+30\ \text{km s}^{-1}$ and undergoes only small changes along the flow. The low values of radial velocities point to the flow propagation near the plane of sky, just as in the case of FS Tau B jet.

Our attention was drawn by the star that lies just near the axis of the flow, namely IRAS F04192+2647 (CFHT-Tau21). This source was classified as a very low-mass star with undoubted outflow signatures, such as near-infrared excess radiation arising from the accretion disk and forbidden lines in the spectrum (Guieu et al. 2006). On the other hand, this source is one of brightest objects in the WISE survey $22\ \mu\text{m}$ map of this region. Our long-slit spectroscopy of this source, carried out at Byurakan Observatory, allowed us to detect an Li I absorption line, which is a further indication of youth of this star.

We propose this star as a probable source of the HH 276 outflow. This study is described in more detail in a separate paper (Movsessian et al. 2019).

4. Conclusions

We have performed two epoch FPI observations of FS Tau A/B region in $H\alpha$ emission, which allowed us to measure the PM of the spectrally separated emission structures in the FS Tau B HH outflow system.

This HH outflow not only narrows with the distance (Mundt et al. 1991), but also demonstrates the strong variations of the width depending on radial velocity. Namely, the optical flow is more narrow in the high radial velocity than in the low velocity channels. In the more distant part of flow, strong variations of morphology are not observed. Such behaviour of the optical flow can be explained by a stronger contribution of oblique shock zones in the low velocity channels.

With the aid of the more deep second epoch data we discovered the new emission structures in the extended part of the jet (knot M2 with the trailing faint bow-shaped structure) and in the counter-jet (knot W). On the other hand, a new relatively bright HH object was discovered in the southeastern direction from FS Tau A/B system. This object lies on the axis of HH 276 flow and is denoted as HH 276E. As a presumable source of this independent flow, the star CFHT-Tau21 with undoubted outflow signatures, described by Guieu et al. (2006), can be considered.

The PMs of the spectrally separated structures were estimated. An especially high PM was detected in the bright bow-shaped knot B. We can conclude that the velocity of the outflow undergoes strong variations in time.

The terminal working surface of the jet undergoes apparent morphological variations depending on radial velocity. Two compact knots (K and L) were detected in high radial velocities, accompanied by two leading bow-shaped low velocity structures. In the case of knot L the structures with different radial velocities have PMs of the same value. This result can be interpreted as the direct observation of bow-shock and Mach disk regions in the terminal working surface. These data lead to the more precise estimations of the inclination to the plane of the sky and the spatial velocity of knot L, which are equal to 12° and $300\ \text{km s}^{-1}$, respectively. On the other hand, significantly dissimilar PMs of knots K and L suggest their interpretation as two separate working surfaces, perhaps created by two independent outbursts.

Aside from moving knots and bright bow-shaped structures, an unusual bar-like structure, which demonstrates zero PM,

exists in the jet and is located to the southwest from the source. It can be yet another example of the deflection shock (Hartigan et al. 2011), which occurs when high velocity wind impacts the edge of the cavity formed by outflow.

Analyses of $H\alpha$ profiles in the R1 reflection nebula and in the point near the invisible source position (R3) reveals their strong difference. Near the source, where we observe the scattered light in the circumstellar disk, the broad emission was detected, while the averaged profile in the R1 nebula splits into two components. A reflection nebula probably works as a mirror and we observe the same object from the edge-on and the pole-on points of view simultaneously, which makes FS Tau B a unique object. The large width of $H\alpha$ line in the position of R3 reflection nebula, in comparison with the emission in FS Tau B jet, can be the result of a wide opening angle of the jet base.

All these results once again demonstrate that the observations with FPI represent a very powerful method for the investigation of extended emission objects, especially if combined with the measurement of the PMs of spectrally separated structures.

Acknowledgements. The authors thank the referee for helpful suggestions. We are grateful to Dr. V.A. Moiseev for very important contributions in observations and data reduction. The authors also thank Dr. J. Eisloffel for providing his observational data and helpful discussions. This work was supported by the RA MES State Committee of Science, in the frames of the research projects number 15T-1C176 and 18T-1C-329.

References

- Afanasiev, V. L., & Moiseev A. V. 2005, *Astron. Lett.*, **31**, 194
 Appenzeller, I., Bertout, C., & Stahl, O. 2005, *A&A*, **434**, 1005
 Cabrit, S., Edwards, S., Strom, S. E., & Strom, K. M. 1990, *ApJ*, **354**, 687
 Cohen, M., & Kuhl, L. V. 1979, *ApJS*, **41**, 743
 Dopita, A. 1978, *A&A*, **63**, 237
 Eisloffel, J., & Mundt, R. 1992, *A&A*, **263**, 292
 Eisloffel, J., & Mundt, R. 1998, *AJ*, **115**, 1554
 Falle, S. A. E. G., & Raga, A. C. 1995, *MNRAS*, **272**, 785
 Guieu, S., Dougados, C., Monin, J.-L., Magnier, E., & Martin, E. L. 2006, *A&A*, **446**, 485
 Haro, G., Iriarte, B., & Chavira, E. 1953, *Bol. Obs. Tonantz. Tacub.*, **1**, 3
 Hartigan, P. 1989, *ApJ*, **339**, 987
 Hartigan, P., & Raymond, J. 1993, *ApJ*, **409**, 705
 Hartigan, P., Raymond, J., & Hartmann, L. 1987, *ApJ*, **316**, 323
 Hartigan, P., Edwards, S., & Ghandour, L. 1994, *BAAS*, **26**, 1389
 Hartigan, P., Morse, J., Palunas, P., Bally, J., & Devine, D. 2000, *AJ*, **119**, 1872
 Hartigan, P., Heathcote, S., Morse, J., Reipurth, B., & Bally, J. 2005, *AJ*, **130**, 219
 Hartigan, P., Frank, A., Foster, J. M., et al. 2011, *ApJ*, **736**, 29
 Jones, B. F., & Herbig, G. H. 1982, *AJ*, **87**, 1223
 Kenyon, S. J., Gómez, M., & Whitney, B. A. 2008, in *Handbook of Star Forming Regions*, ed. B. Reipurth (US: Astronomical Society of the Pacific), I, 405
 Kirchschlager, F., Wolf, S., & Madlener, D. 2016, *MNRAS*, **462**, 858
 Krist, J. E., Stapelfeldt, K. R., Burrows, C. J. et al. 1998, *ApJ*, **501**, 841
 Kurosawa, R., Harries, T. J., & Neil, H. S. 2006, *MNRAS*, **370**, 580
 Moiseev, A. V. 2002, *Bull. Spec. Astrophys. Obs.*, **54**, 74
 Moiseev, A. V., & Egorov, O. V. 2008, *Bull. Spec. Astrophys. Obs.*, **63**, 181
 Morse, J. A., Hartigan, P., Cecil, G., Raymond, J. C., & Heathcote, S. 1992, *ApJ*, **399**, 231
 Morse, J. A., Heathcote, S., Cecil, G., Hartigan, P., & Raymond, J. C. 1993, *ApJ*, **410**, 764
 Mottram, J. C., Van Dishoeck, E. F., Kristensen, L. E., et al. 2017, *A&A*, **600**, A99
 Movsessian, T. A., Magakian, T. Yu., Amram, P., Boulesteix, J., & Gach, J.-L. 2000, *A&A*, **364**, 293
 Movsessian, T., Magakian, T. Yu., Bally, J. 2007, *A&A*, **450**, 605
 Movsessian, T. A., Magakian, T. Yu., Moiseev, A. V., & Smith, M. D. 2009, *A&A*, **508**, 773
 Movsessian, T., Magakian, T. Yu., & Moiseev, A. V. 2012, *A&A*, **541**, A16
 Movsessian, T., Magakian, T. Yu., & Moiseev, A. V. 2014, Protostars and Planets VI, Heidelberg, July 15-20, 2013. Poster #1K038
 Movsessian, T., Magakian, T. Yu., & Gevorgyan, M. A. 2019, *Astrophysics*, **62**, 35
 Mundt, R., Bührke, T., Fried, J. W., et al. 1984, *A&A*, **140**, 17
 Mundt, R., Brugel, E. W., & Bührke, T. 1987, *ApJ*, **319**, 275
 Mundt, R., Ray, T., & Bührke, T. 1988, *ApJ*, **333**, L69
 Mundt, R., Ray, T. P., Bührke, T., Raga, A. C., & Solf, J. 1990, *A&A*, **232**, 37
 Mundt, R., Ray, T. P., & Raga, A. C. 1991, *A&A*, **252**, 740
 Padgett, D. L., Brandner, W., Stapelfeldt, K. R., et al. 1999, *AJ*, **117**, 1490
 Raga, A. C., Canto, J., Binette, L., & Calvet, N. 1990, *ApJ*, **364**, 601
 Ray, T. P., Mundt, R., Dyson, J. E., Falle, S. A. E. G., & Raga, A. C. 1996, *ApJ*, **468**, L103
 Reipurth, B. 1989, *A&A*, **220**, 249
 Reipurth, B., & Heathcote, S. 1992, *A&A*, **257**, 693
 Reipurth, B., Raga, A. C., & Heathcote, S. 1992, *ApJ*, **392**, 145
 Reipurth, B., Hartigan, P., Heathcote, S., Morse, J., & Bally, J. 1997, *AJ*, **114**, 757
 Rodríguez, L. F., Cantó, J., Torrelles, J. M., Gómez, J. F., & Ho, P. T. P. 1992, *ApJ*, **393**, L29
 Rodríguez, L. F., Cantó, J., Torrelles, J. M. 1994, *ApJ*, **427**, L103
 Stapelfeldt, K., Burrows, C. J., Krist, J. E., & the WFPC2 Science Team 2016, in Herbig-Haro Flows and the Birth of Low Mass Stars, eds. B. Reipurth & C. Bertout (Dordrecht: Kluwer), *IAU Symp.* **182**, 355
 Stone, J. M., & Norman, M. L. 1993, *ApJ*, **413**, 210
 Wilner, D. J., Ho, P. T. P., & Rodríguez, L. F. 1996, *ApJ*, **470**, L117
 Woitas, J., Eisloffel, J., Mundt, R., & Ray, T. P. 2002, *ApJ*, **564**, 834
 Yokogawa, S., Kitamura, Y., Momose, M., et al. 2001, *ApJ*, **552**, L59